# Diurnal Variation of Outgoing Longwave Radiation in the Tropics

DENNIS L. HARTMANN AND ERNEST E. RECKER

*Department of Atmospheric Sciences, AK-40, University of Washington, Seattle, WA 98195*

(Manuscript received 13 June 1985, in final form 18 November 1985)

ABSTRACT

The diurnal harmonic in longwave emission in the tropical belt (30°N–30°S) is estimated from nine years of NOAA polar-orbiting satellite data. The results are compared successfully with Nimbus-7 ERB scanner data and with GOES-West geosynchronous satellite data. An interesting and consistent diurnal variation in longwave emission is found over the regions of intense oceanic convection such as the ITCZ and SPCZ regions with a peak-to-peak variation of 6–8 W $m^{-2}$ and a maximum in the morning (0600–1200 LST). Histogram analysis indicates that this variation is associated with a diurnal variation in convective cloud (~400 mb). Over regions of very intense convection, a diurnal variation of very high clouds (~100 mb), which is out of phase with the variations at lower levels in the atmosphere, reduces the magnitude of the diurnal harmonic in longwave emission.

It is interesting that histograms based on data averaged over 8-km and 250-km boxes give the same qualitative information about cloud and emission variability.

## 1. Introduction

Within the tropics, large diurnal variations in cloudiness and precipitation are commonly observed, especially over the continents. Diurnal variations in outgoing longwave radiation can serve as a proxy measure of cloudiness and precipitation, since reduced longwave emission from the tropics generally occurs in association with rain-producing clouds. In addition, since the outgoing longwave radiation is one of the two terms in the Earth's energy balance, its diurnal variation is of interest in itself. Because geosynchronous satellites observe only restricted geographical regions, and polar-orbiting sun-synchronous satellites observe at only two local times, the global distribution of the diurnal variation in longwave emission is not well known.

Raschke and Bandeen (1970) presented global maps of the noon minus midnight difference in longwave emission, which showed large positive differences over the land areas. Short and Wallace (1980) presented 0900–2100 LST difference maps for longwave emission based on NOAA satellite observations during June, July, August (JJA) 1975 and December, January, February (DJF) 1975/76. These maps showed large differences over land and nearshore areas that were consistent with diurnal heating of the land surface and diurnal modulation of stratus cloudiness. Over the tropical oceans, the morning to evening differences in emission were small, but histograms showed some consistent differences which suggested a diurnal variation in cloud type.

In this study, we have used data from satellites in sun-synchronous orbits with four different equator crossing times of 0730, 0900, 0230 and 0330 LST. Since the equator crossing times for a single satellite are 12 h apart at a given geographical position, we can combine data taken in different years to estimate the amplitude and phase of the first diurnal harmonic even though substantial interannual variations in longwave emission occur. It is assumed that the first diurnal harmonic includes most of the diurnal variation, although under some conditions this assumption is known to be poor. The accuracy of the estimate of the diurnal harmonic obtained in this manner is tested by comparing the noon–midnight difference map based on our diurnal harmonic with the noon–midnight difference measured directly by the Nimbus-7 ERB scanner.

An interesting feature of the diurnal variation in longwave emission is the variation associated with convective clouds over the ocean. Analysis of histograms of polar orbiter and GOES-West data indicates that the diurnal variation in longwave emission results from a substantial variation in midtropospheric convective cloud (~400 mb tops) with minimum cloudiness occurring in the late morning or near noon. In regions of intense deep convection, the diurnal variation in longwave radiation that would result from the midlevel cloud is partially offset by a diurnal variation of very high clouds that is 180° out of phase with that of the cloud in the midtroposphere.

## 2. Data and analysis

Nearly ten years of outgoing longwave and albedo data collected by NOAA sun-synchronous satellites and archived at 2.5 × 2.5 degree resolution are available. The data are archived separately for the ascending and descending nodes of the orbit, which can be related to

two local times at which the satellite crosses the equator. Table 1 presents the satellites, the observation periods and the local times for the data used in this study. Because longwave data are available for four separate orbits, giving eight different local times, it is possible to determine the amplitude and phase of the diurnal harmonic. Near the equator, each satellite samples local times that are 12 h apart; thus, interannual variations in the daily mean longwave radiation do not affect estimates of the diurnal harmonic. Because the interannual variability in the diurnal average exitance is large, it is not possible to separate the semidiurnal harmonic from the interannual variations in the diurnal mean. For the same reason, attention must be limited to the tropical strip where the ascending and descending nodes are approximately 12 h apart.

The eight local times that are available are not evenly spaced throughout the day, so a regression procedure, rather than a Fourier transform, must be used to obtain the coefficients of a harmonic expansion of the form

$$F(t) = \sum_{n=0}^{N} a_n f_n(t) \tag{1}$$

where $a_n$ are coefficients to be determined and the basis functions are

$$f_n(t) = \{1, \cos 2\pi t, \sin 2\pi t, \cos 4\pi t, \sin 4\pi t, \cdots\} \tag{2}$$

where $t$ is given in days. To obtain the coefficients, we require that the mean square error be minimized:

$$Q = \frac{1}{T}\sum_{i=1}^{T}[x(t_i) - \sum_{n=0}^{N} a_n f_n(t_i)]^2$$

$$= \overline{[x(t_i) - \sum_{n=0}^{N} a_n f_n(t_i)]^2}, \tag{3}$$

where the $t_i$ are those times of day at which we have observations. Defining the covariance matrix between the basis functions:

$$C_{nm} = \overline{f_n(t_i) f_m(t_i)} \tag{4}$$

and the covariance vector between a particular basis function and the data to be fit

$$V_m = \overline{x(t_i) f_m(t_i)}\,, \tag{5}$$

we obtain the solution for the minimization of (3) in the form

$$a_n = C_{mn}^{-1} V_m. \tag{6}$$

If the data are evenly spaced, then $C_{mn}$ becomes a diagonal matrix and we recover the formula for a Fourier transform. It is efficient to use (6) for large data sets since $C_{mn}^{-1}$ need be calculated only once and the calculation of the vector $V_m$ requires only $T = 8$ multiplications and additions per data point. The $x(t_i)$ here are the climatological seasonal averages for a particular time of day, $t_i$.

TABLE 1. NOAA longwave radiation data used in this study.

| Satellite | Time of equator crossing | Period of record | Months of data |
|---|---|---|---|
| NOAA-2, 3, 4, 5 | 0900–2100 LST | Jun 1974–Feb 1978 | 45 |
| TIROS-N | 0330–1530 LST | Jan 1979–Jan 1980 | 13 |
| NOAA-6 | 0730–1930 LST | Feb 1980–Aug 1981 | 17 |
| NOAA-7 | 0230–1430 LST | Sep 1981–Nov 1983 | 27 |

## 3. The diurnal harmonic of outgoing longwave radiation

### *a. Diurnal harmonic based on NOAA data*

The amplitude and phase of the diurnal harmonic, determined by the method described in the previous section, is presented in Fig. 1 for each of four three-month seasons. The structure of the amplitude of the diurnal harmonic is shown in the form of contours at 2, 5, 10 and 20 W m$^{-2}$. The lengths of the arrows are constant for amplitudes greater than 5 W m$^{-2}$ and decrease linearly for amplitudes less than 5 W m$^{-2}$. Arrows are not shown for amplitudes less than 1 W m$^{-2}$. The contour value is thus easily determined by beginning at the 2 W m$^{-2}$ contour bordering a region with missing arrows and counting contours in the direction of increasing arrow length. It is immediately apparent that the amplitude is largest over the land, especially over desert areas. Significant amplitudes also appear over the oceans far from land, however.

The phase of the diurnal harmonic is indicated by arrows. An arrow pointing south indicates a maximum in longwave radiation at 1200, eastward at 0600, northward at 2400 and westward at 1800 LST. Over dry land areas the amplitude is large and the maximum longwave emission occurs near noon. In highly convective regions over the tropical continents, the amplitude of the diurnal harmonic is reduced. Over South America during the equinoctial seasons, the maximum occurs before noon. This phase shift is consistent with an afternoon maximum in convective activity over the Amazon Basin. Minnis and Harrison (1984c) have shown that about two-thirds of the diurnal variation of longwave exitance over the Amazon Basin is associated with varying cloud-top altitudes. The highest average cloud-top altitude occurs in the late afternoon or evening.

West of South America and southern Africa, large regions with afternoon maxima in emission can be seen. These are best developed during the Austral summer (DJF). A similar region can be seen to the west of northern Africa during the JJA season. These are regions of low stratiform cloud in which the cloud coverage is greatest in the early morning.

The aforementioned features and the complex structure around the Indonesian Islands were apparent in the 0900–2100 difference maps of Short and Wallace

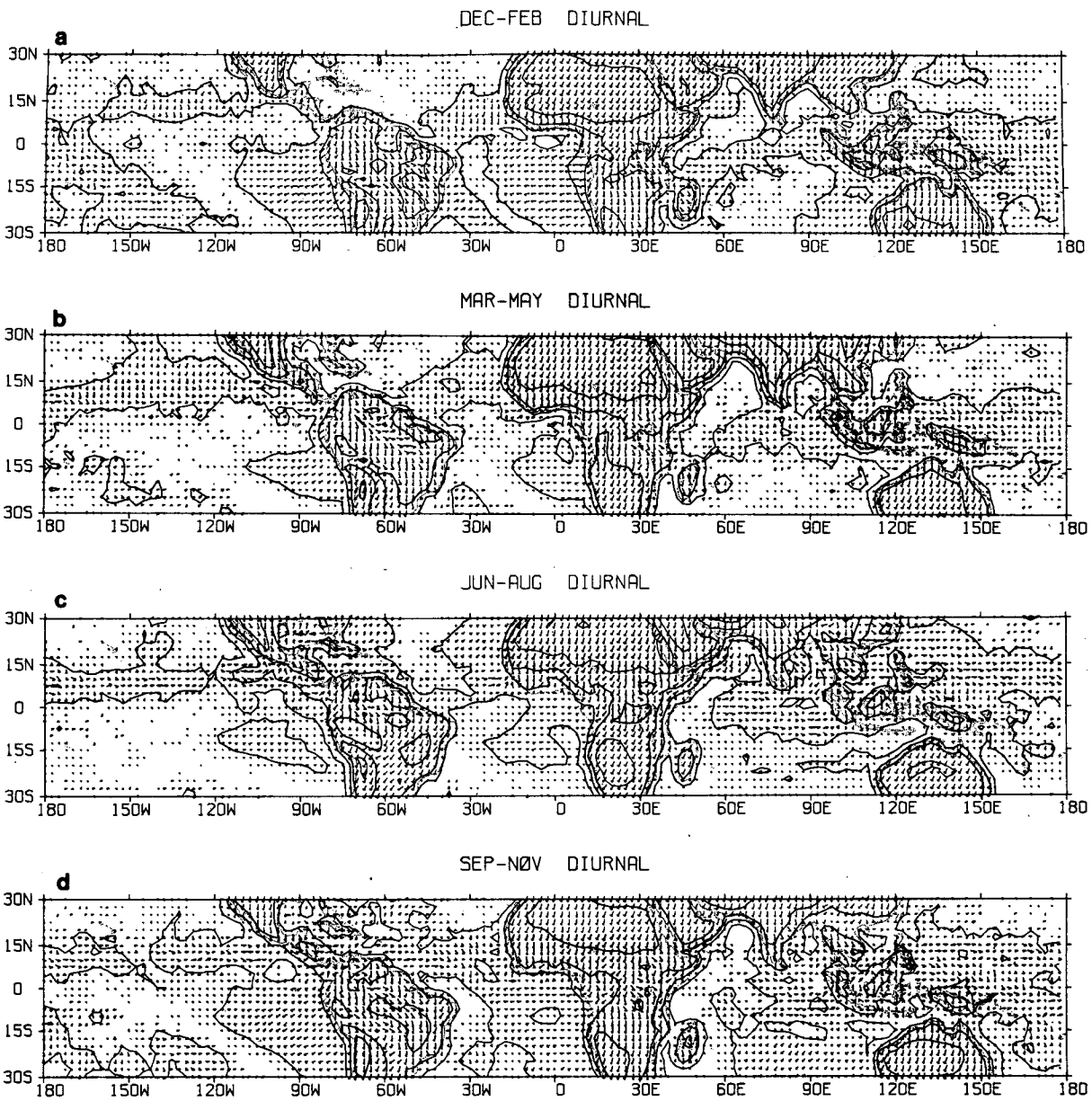


FIG. 1. Amplitude and phase of the first harmonic of the diurnal variation in longwave exitance inferred from NOAA-4 (0900–2100 LST), TIROS-N (0330–1530 LST), NOAA-6 (0730–1930 LST) and NOAA-7 (0230–1430 LST) sun synchronous satellites for the 3-month seasons of (a) December–February, (b) March–May, (c) June–August, (d) September–November. Contours of amplitude are 2, 5, 10 and 20 W $m^{-2}$. The arrows indicate the phase of the diurnal harmonic. Northward pointing arrows indicate maximum longwave emission at midnight; eastward, 0600; southward, noon; and westward 1800 local standard time. When the amplitude is less than 1 W $m^{-2}$ the arrows are not plotted. The arrow length increases linearly with amplitude between 1 and 5 W $m^{-2}$ and remains constant for amplitudes greater than 5 W $m^{-2}$.

(1980). What are apparent in Fig. 1, but not visible in the figures of Short and Wallace, are regions over the open oceans far from land masses where significant diurnal variations appear. These are generally seen in areas where well-developed convection is prevalent, such as the intertropical convergence zone (ITCZ), the South Pacific convergence zone (SPCZ) and the South Atlantic convergence zone (SACZ). In these regions, two preferred phases seem to occur. In the ITCZ region over both the Atlantic and Pacific oceans, the maximum longwave tends to occur near noon during the DJF season. In the same regions during the JJA season, however, the maximum emission occurs earlier in the day, with a preference for a 0600 LST maximum. In general, it seems that the 0600 LST maximum appears at those locations and seasons for which the convection

is strongest. The noon maximum occurs in regions where deep convection is present, but perhaps not so intense. The primary example of this is in the ITCZ region, which is weaker in DJF and shows a noon maximum during that season. In contrast, during JJA, when the ITCZ in the Northern Hemisphere is intense and well developed, the maximum emission tends to occur around 0600. Intermediate seasons often show a mixture of these phases.

The South Atlantic convergence zone (near 25°S, 30°W) shows a consistent 0300 to 0600 LST maximum during the DJF and March, April, May (MAM) seasons. Similar phases also appear in the SPCZ during these seasons, although less consistently.

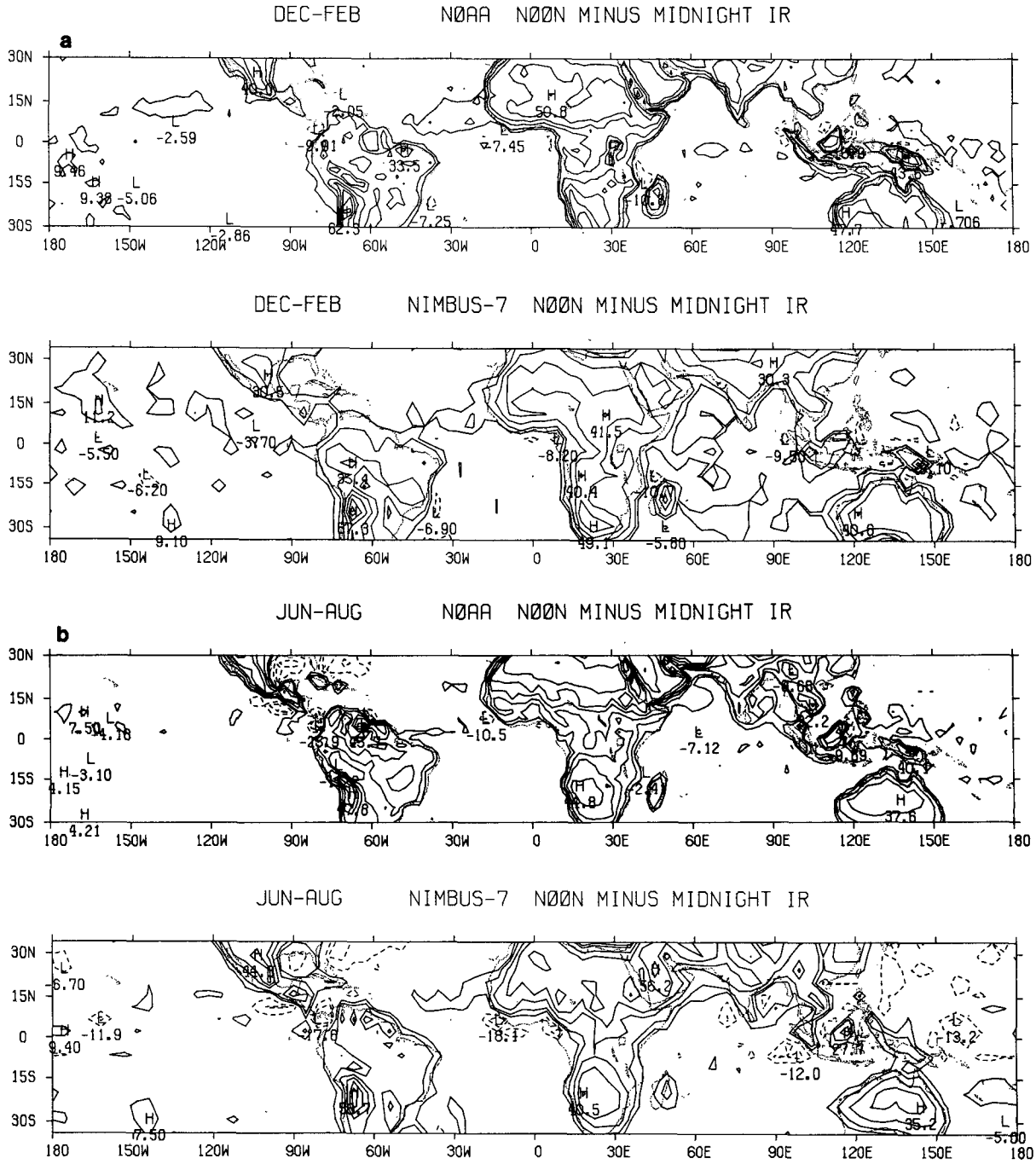


FIG. 2. Noon minus midnight differences in longwave exitance inferred from the data presented in Fig. 1 (top) and noon minus midnight differences measured directly by the Nimbus-7 ERB scanner (bottom) for (a) the DJF season and (b) the JJA season. Contour intervals are 5, 10, 20, 30, 40, 50, 60 W $m^{-2}$. Negative contours are dashed.

*b. Comparison with Nimbus-7 ERB data*

To test the procedure used to calculate the diurnal harmonic, we have compared the noon–midnight differences implied by our diurnal harmonic with those observed directly by the Nimbus-7 ERB scanner (e.g., Jacobowitz et al., 1984). The results for the solstitial seasons are shown in Fig. 2. There are several important differences in the two inferences of noon–midnight differences which need to be considered:

1) The NOAA noon minus midnight difference was inferred from the diurnal harmonic based on the local times shown in Table 1. None of these times is closer than 2.5 h to a noon–midnight orbit. The Nimbus-7 difference was measured directly from a noon orbit.
2) The NOAA longwave emission was inferred by regression from observations taken in a narrow frequency band in the 11 $\mu$m water vapor window (roughly 10–12 $\mu$m, but the frequency response varies slightly from instrument to instrument; Gruber and Krueger, 1984). The Nimbus-7 data are based on a direct broadband measurement of the Earth's emission (>4 $\mu$m).
3) The NOAA data are archived with better (2.5° × 2.5°) horizontal resolution than the Nimbus-7 data (4.5° × 4.5° and 4.5° × 5.0° in the region we are considering).
4) The NOAA estimate of the difference is based on data taken over a 9-year period as indicated in Table 1. Nimbus-7 data are from an 18-month period starting in November 1978.

In comparing the panels in Fig. 2, the most apparent of the four differences cited above is the difference in spatial resolution. The maxima in the differences seem to be larger in the NOAA data, but this may be due as much to spatial resolution as to any other potential cause. During the DJF season, both the NOAA and Nimbus-7 difference maps show positive values in the ITCZ region, especially in the Atlantic. This is consistent with the noon maximum shown in Fig. 1. During JJA, these differences are reduced. Figure 1 suggests that this is not because diurnal variations are not pres-

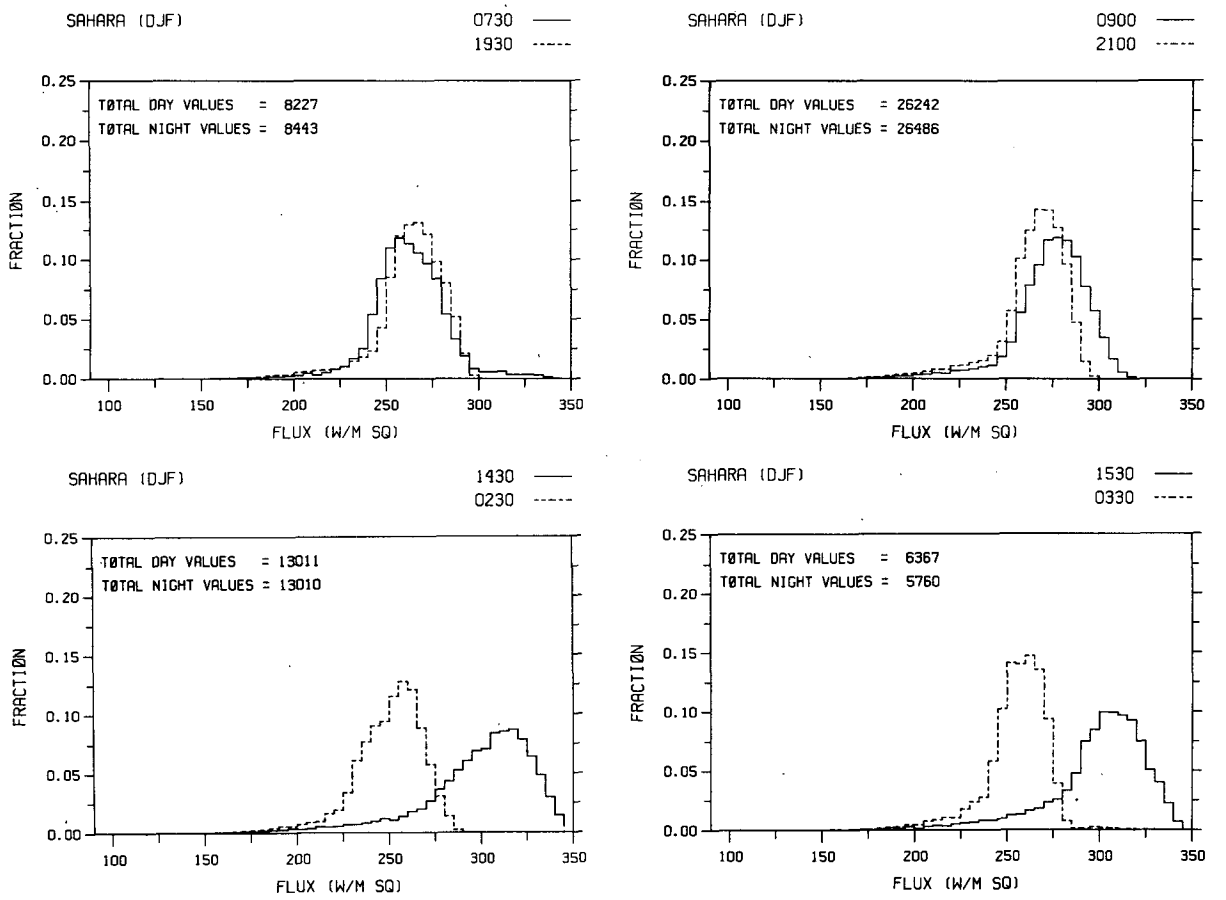


FIG. 3. Histograms of the frequency of occurrence of instantaneous longwave exitances from 2.5° × 2.5° grid squares for the DJF season in the Sahara Desert region at each local time. (0730–1930 LST, upper left; 0900–2100 LST, upper right; 0230–1430 LST, lower left; 0330–1530 LST, lower right.) Daytime histograms are shown in solid lines; nighttime histograms are shown in dashed lines.

ent, but rather because the maximum and minimum longwave occur near 0600 and 1800 LST so that little signal is seen in a noon–midnight difference map because noon and midnight are near the nodes of the oscillation.

### c. *Histogram analysis*

Histograms of the individual daily observations in a grid square can be used to determine what sort of variations lead to the diurnal variations in longwave emission. Figure 3 shows histograms for each of the local times over the Sahara Desert during the DJF season. The differences between the local times result primarily from surface temperature variations over the desert. At 0900 LST, the surface temperature and the longwave emission are slightly larger than at 2100 LST. The difference between the 0330 and 1530 LST histograms is much greater, with the afternoon emission being much larger. It is clear that the change in the mean emission results from a shift in the position of the distribution, rather than only a change in its shape. This is indicative of large changes in surface temperature. (See also Duvel and Kandel, 1985.) Figure 4 shows the histograms for the region west of South America during DJF where stratus cloudiness is prevalent. In this case, the histogram is very narrow and the diurnal variations result from changes in the shape of the distributions. At 1530 LST the histogram is peaked near the largest values of emission. This suggests a greater occurrence of clear skies over the ocean. In the early morning hours at 0330 LST the histogram is peaked more toward the central or lower values of the emission, suggestive of a greater fractional coverage by low clouds. The inferences derived from Fig. 4 are consistent with the analyses of hourly, high spatial resolution geosynchronous observations for November 1978 by Minnis and Harrison (1984a–c). They found that the total cloudiness in the stratus region west of South America, which was dominated by low stratus cloud, reached a maximum in the early morning hours (0300–0600 LST) and a minimum in the midafternoon (~1530 LST). The forcing mechanism for these diurnal variations in low stratiform cloud is the diurnal variation of solar heating in the cloud as described, for example, by Fravalo et al. (1981).

The histograms for the ITCZ region show a much broader distribution of emission values than the stratus

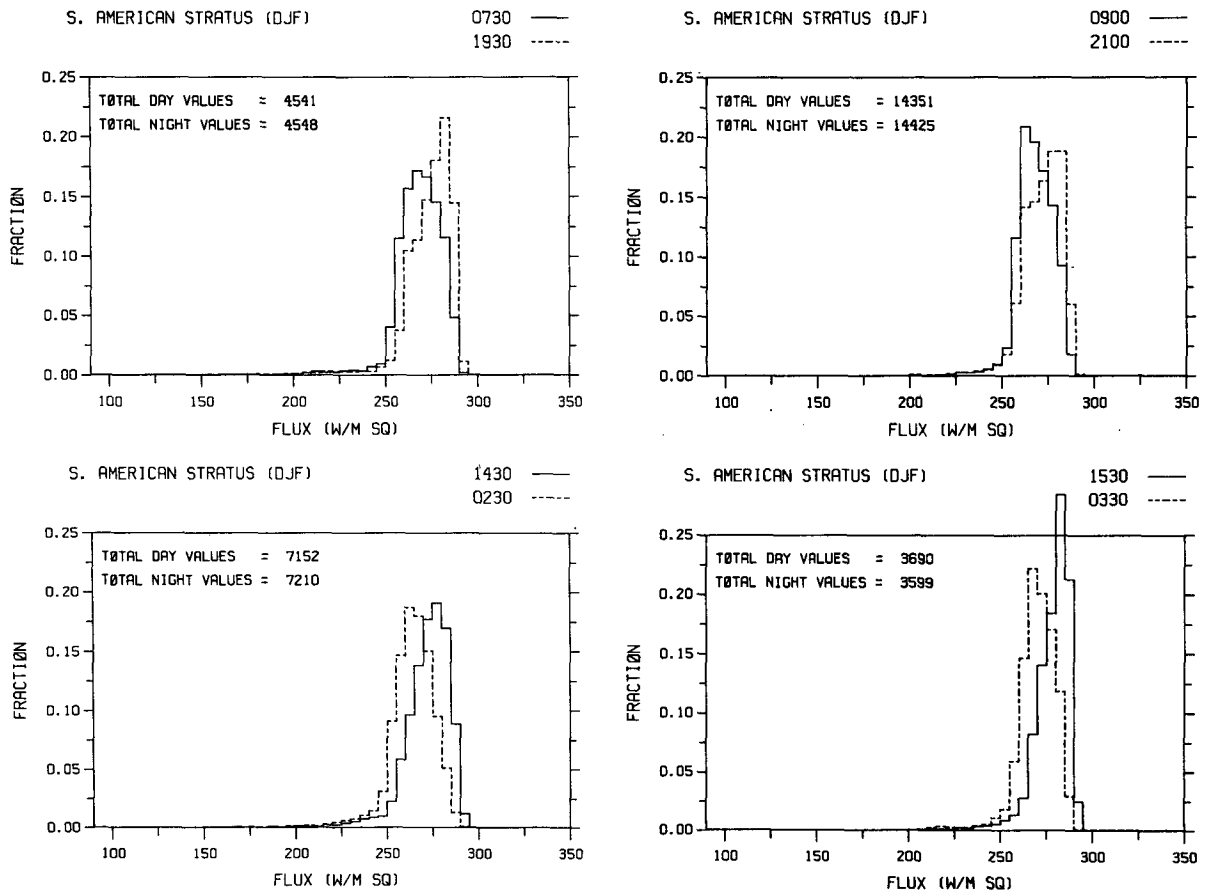


FIG. 4. As in Fig. 3 except for the region of stratus cloudiness over the southeastern Pacific Ocean west of South America.

or desert regions. Figure 5 shows the histograms in the Pacific ITCZ region for the JJA season. The top two panels show that in the evening (1930 and 2100 LST), more occasions with emissions in the 200 W $m^{-2}$ region occur than in the morning (0730 and 0900 LST) and fewer occasions with emissions in the 275–300 W $m^{-2}$ region are seen. This suggests that there are more middle level clouds in the evening than in the morning. The fact that the compensating differences in the fractional coverage occur in the region of the largest values of emission suggests that when the middle level clouds are absent they are replaced by clear sky or very low clouds. The 0900–2100 LST difference reverses for very low emissions (~130 W $m^{-2}$), as previously noted by Short and Wallace (1980), but this crossover is not so apparent in the data for the other orbits. The crossover at low values of exitance in the 0900–2100 differences suggests that very high clouds occur more frequently in the morning than in the evening, but their contribution to the diurnal variation in total longwave emission is probably smaller than the more commonly occurring midlevel cloud.

It is interesting that the largest differences between day and night histograms occur at higher altitudes for the afternoon versus early morning comparisons (0230 and 0330 LST orbits) than for the morning versus evening comparisons (0730 and 0900 LST orbits). The main crossover point in the histograms occurs near 200 W $m^{-2}$ for the 0230 and 0330 LST orbits but near 250 W $m^{-2}$ for the 0730 and 0900 LST orbits. A shift with altitude of the phase of the diurnal harmonic in cloudiness is suggested by this feature of Fig. 5. Further corroboration will be provided in section 3d with data from a geosynchronous satellite.

The histograms for the Pacific ITCZ region during the DJF season (Fig. 6) are peaked more strongly at high values of the emission than are those of the JJA season. This difference of histogram shape suggests fewer deep convective clouds and more clear sky occurrences during the DJF season, which is consistent with expectation. During DJF the 0900–2100 LST and 0330–1530 LST comparisons show more midlevel cloudiness during the afternoon and evening hours, giving rise to the weak noontime maximum in longwave emission shown in Fig. 1. Because of the smaller sample size for the 0330–1530 LST orbit, the histograms for those local times are generally noisier than those for the 0900–2100 LST orbit. Similar results to

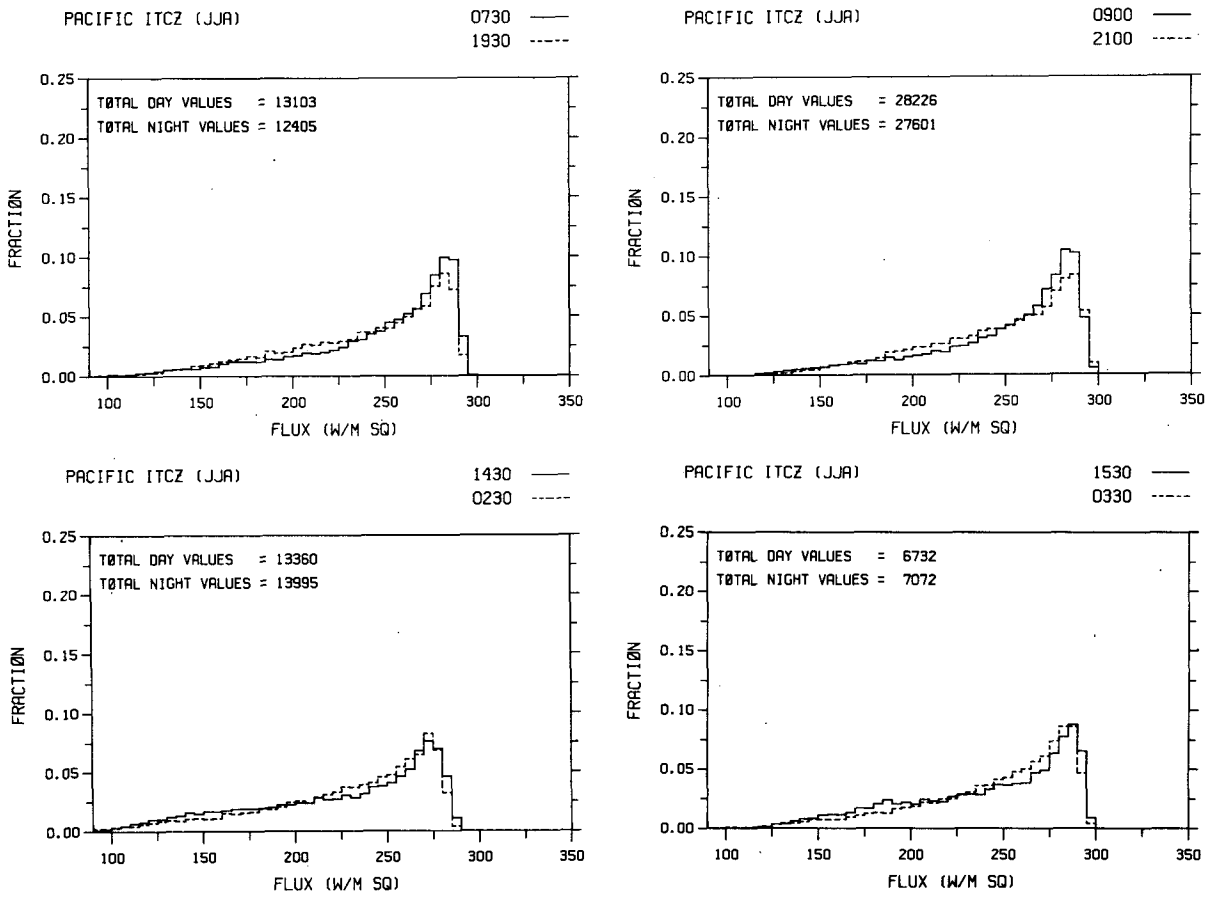


FIG. 5. As in Fig. 3 except for the region of the ITCZ over the Pacific Ocean during the JJA season.

those shown in Fig. 6 have been obtained for the Atlantic ITCZ during the DJF season (not shown).

Figure 6 gives some indication of the interannual variability in the Pacific ITCZ region during DJF. In the previous example for the JJA season the 0730 and 0900 LST orbits and the 0230 and 0330 LST orbits gave similar histograms, as one would expect because of their proximity in time. During DJF, however, the ITCZ is normally very weak unless an El Niño event is in progress. El Niño events occurred during 1976–77 and 1982–83 when the sea surface temperatures (SST) in the eastern Pacific were warmer than normal. These years are included in the periods covered by the 0900 and 0230 LST orbits, respectively. High SST are normally accompanied by an increase in the amount of high cloud (e.g., Liebmann and Hartmann, 1982). As a result, the histograms for the 0900 and 0230 LST orbits are less skewed toward high values of the longwave emission than are the samples for periods with no warm SST events included (the 0730 and 0330 LST orbits).

Figure 7 shows the histograms taken from the South Atlantic convergence zone during the DJF season. For the 0730–1930 LST and 0900–2100 LST comparisons the differences are rather small but with a tendency for more middle level cloudiness in the evening. The 0230–1430 LST and 0330–1530 LST comparisons show a tendency for more upper-level cloud to be present in the afternoon (1530) than in the early morning (0330). This clearly gives rise to the consistent 0300–0600 longwave emission maximum shown in Fig. 1a. Similar results are presented in Fig. 8 for the South Pacific convergence zone during DJF.

### *d. Comparison with geosynchronous satellite data*

Albright et al. (1985) have shown that substantial diurnal variations in cloud type occurred over the Pacific Ocean during the January–February 1979 period. In this section, the implications of these cloud type variations for the top-of-atmosphere longwave exitance will be investigated and compared with the results of our analysis of the diurnal harmonic in the NOAA data. We are interested to see how well our histograms of 2.5° × 2.5° averages compare qualitatively with histograms of fine spatial resolution data. In addition, the geosynchronous data are available every three hours, so that we can see how well the diurnal variation in

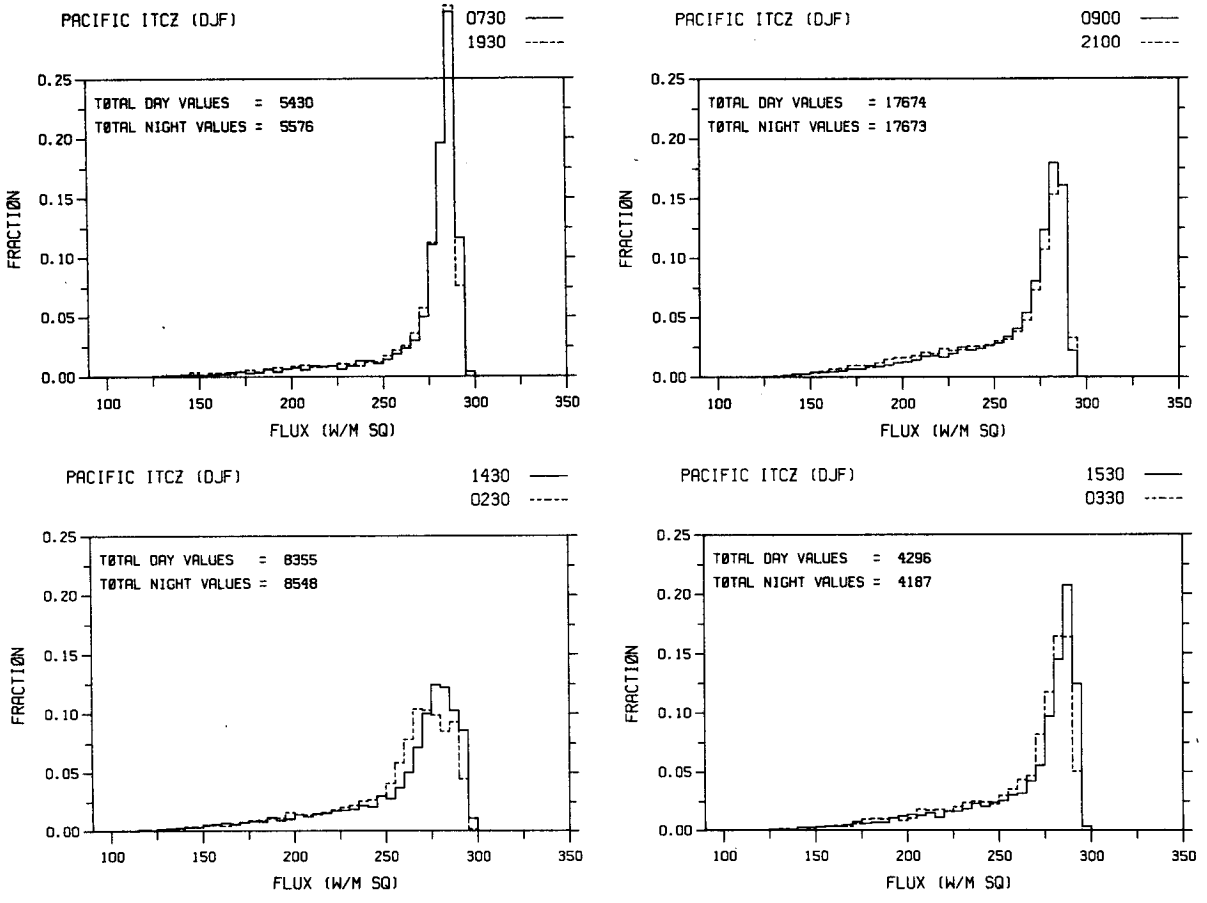


FIG. 6. As in Fig. 5 except for the DJF season.

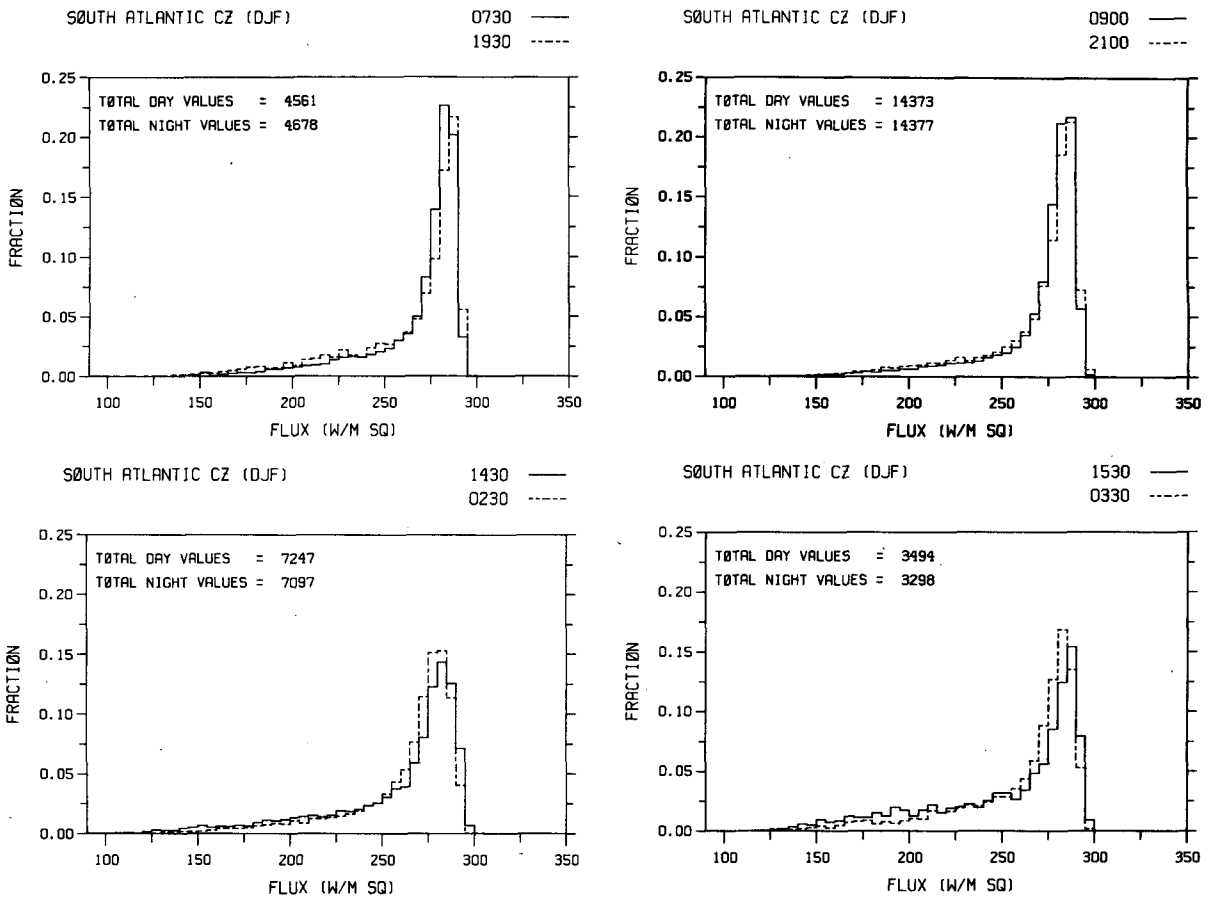


FIG. 7. As in Fig. 3 except for the South Atlantic convergence zone region during the DJF season.

longwave emission over the ocean is modeled with a single diurnal harmonic.

The GOES-West data used in this section are based on the individual IR pixels which have a spatial extent of about 4 km in the east–west direction and 8 km in the north–south direction. Figure 9 shows contour plots of the diurnal variation of the percent of an area with equivalent blackbody temperatures warmer than a particular value which is occupied by regions with temperatures within 0.5 K of that value. The quantity plotted in Fig. 9 can be written symbolically as

$$P'(T^*|T \geq T^*, t) = P(T^*|T \geq T^*, t) - \bar{P}(T^*|T \geq T^*) \quad (7)$$

where

$$P(T^*|T \geq T^*, t) = \frac{N[T^* - 0.5\text{ K} < T(t) \leq T^* + 0.5\text{ K}]}{N[T(t) > T^* - 0.5\text{ K}]}. \quad (8)$$

The overbar represents a diurnal average and a prime the deviation from the diurnal average; $N[T_1 < T(t) \leq T_2]$ is the total number of pixels at local time $t$ with temperatures satisfying the inequality inside the parenthesis; $P$ can be interpreted as a conditional probability. It is the probability that the emission temperature is within $T^* \pm 0.5$ K, given that it is greater than $T^* - 0.5$ K.

This quantity is different from that of Albright et al. (1985) who plotted an unconditioned probability

$$P(T^*, t) = \frac{N[T^* - 0.5\text{ K} < T(t) \leq T^* + 0.5\text{ K}]}{N_0(t)} \quad (9)$$

where $N_0(t)$ is the total number of pixels in the sample at local time $t$. In regions with substantial cloudcover the distinction between (8) and (9) is very important. The latter form will always show an apparent variation in low-level clouds in association with a variation in upper-level clouds simply because of the obscuration of warm scenes by cold clouds. On the other hand, (8) will indicate a variation in low-level clouds only if such a variation has actually been observed. The difference between (8) and (9) is particularly important if one wishes to diagnose the contributions by various cloud types to the diurnal variation in longwave emission. We have calculated the contribution to the diurnal

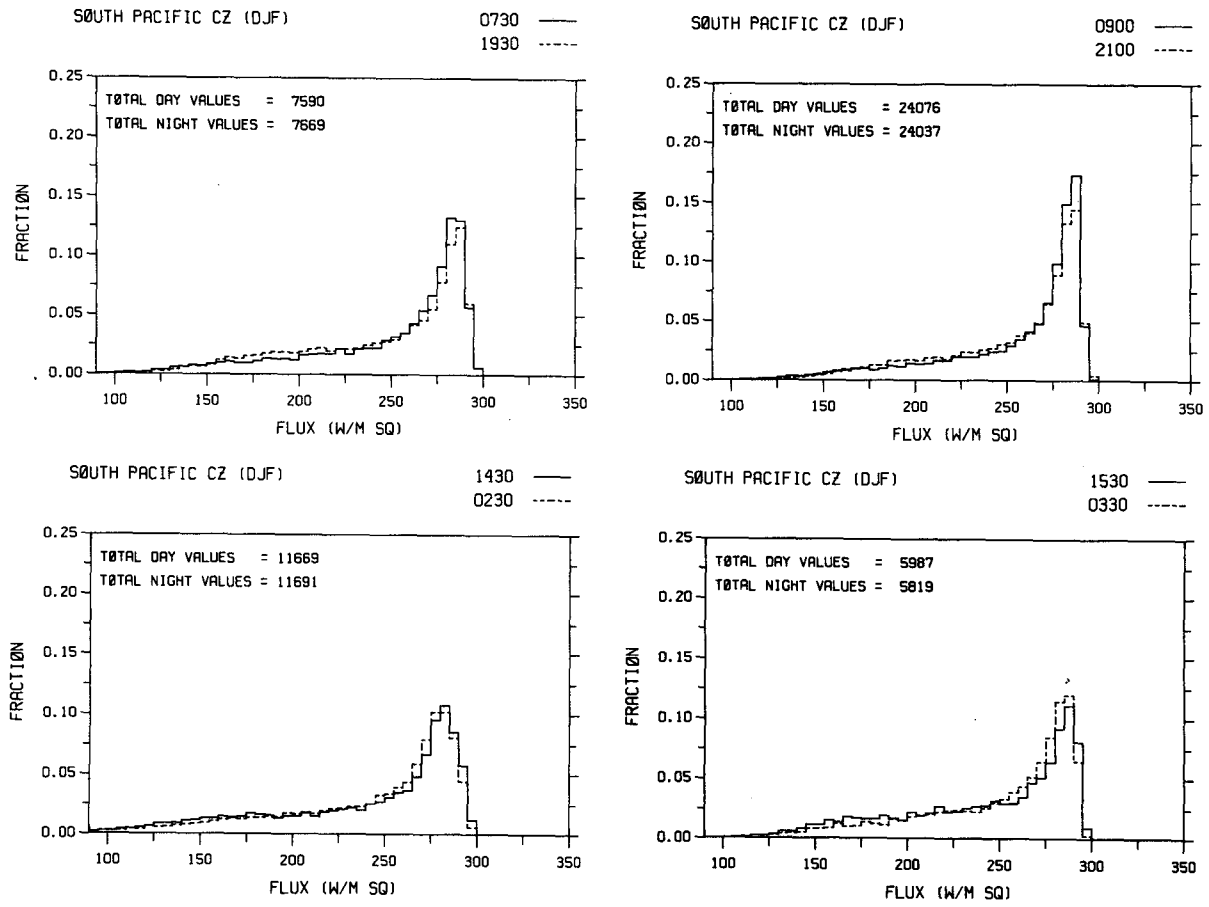


FIG. 8. As in Fig. 3 except for the South Pacific convergence zone during the DJF season.

variation in longwave emission by clouds with tops warmer than a particular value using the following formula:

$$F(T^*, t) = \frac{\sum_{T^*}^{\infty} \sigma T^{*4} P(T^* | T \geq T^*, t)}{\sum_{T^*}^{\infty} P(T^* | T \geq T^*, t)}. \quad (10)$$

Figure 10 shows $F(T^*, t)$ as given by (10). Note that (10) will overestimate the magnitude of the diurnal variation, since the temperatures are equivalent blackbody temperatures in the water vapor window and absorption by atmospheric gases at other frequencies has not been taken into account.

The regions considered in this analysis of GOES-West data are described in Table 2 and in Albright et al. (1985). We show results for the South Pacific convergence zone (SPCZ), which is very active during the Southern Hemisphere summer season we are considering, and for the intertropical convergence zone (ITCZ), which is comparatively suppressed.

In the SPCZ-West (region 1) and SPCZ-East (region 2) regions, where very active convection is present during January and February, Fig. 9 shows clear evidence of strong diurnal variations in upper-level cloudiness. The strongest variability in the region above 700 mb in the SPCZ-West region is centered at about 400 mb. At this level the minimum in cloudiness occurs shortly before noon and the maximum at about 2100 LST. The phase of this diurnal variation becomes earlier in the day with increasing altitude so that near 700 and 100 mb the oscillation appears with reversed phase from that at 350 mb. The amplitude of the diurnal variation has minima in the vicinity of rapid phase variations near 600 and 175 mb.

In the SPCZ-East region, which is both to the east and slightly equatorward of the SPCZ-West region, a somewhat similar pattern appears in the 600–200 mb region, but the reversed phase oscillations at 700 and 100 mb are much less pronounced. The maximum amplitude is now above 300 mb where there is a very pronounced semidiurnal component to the cloudiness variation.

In the Pacific ITCZ region (regions 3 and 6) during the January–February 1979 period, large diurnal variations are confined below 350 mb (Fig. 9). During this season the convection in the ITCZ is not as well-de-

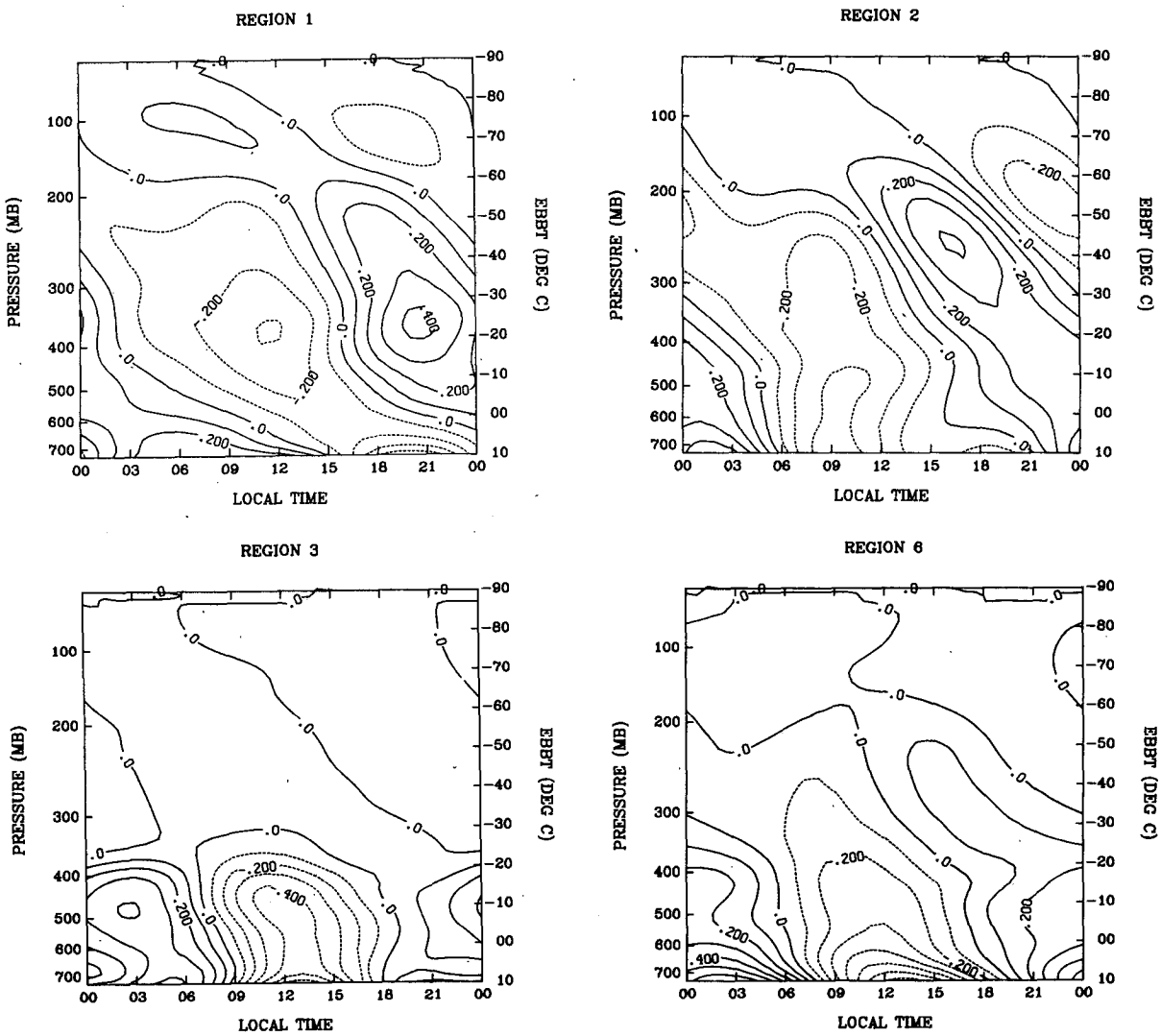


FIG. 9. Deviation from the diurnal average of the ratio of the number of GOES-West IR pixels with equivalent black-body temperatures in 1°C intervals to the number of GOES-West pixels with a black-body temperature equal to or greater than that value. Contours of 0.1% (0.001) are plotted on a grid of local time vs blackbody temperature. Negative deviations from the diurnal average are indicated by dashed contours. The region numbers correspond to those used by Albright et al. (1985). Region 1 is the SPCZ-West, region 2 is the SPCZ-East, region 3 is the Pacific ITCZ-East and region 6 is the Pacific ITCZ-West region.

veloped as that in the SPCZ-West region or that in the ITCZ during JJA.

It is interesting to ask how the diurnal variations in cloudiness apparent in Fig. 9 contribute to the diurnal variation in longwave emission. Figure 10 shows the diurnal variation of the longwave emission which would occur if an average is taken over only those areas with equivalent blackbody temperatures greater than a specified value as given by (10).

In the SPCZ-West region (region 1), the diurnal variation in longwave radiation grows to a maximum amplitude of about 10 W $m^{-2}$ at 200 mb from a very small amplitude at the surface where sea surface temperatures are nearly constant through the day. Above 200 mb, the diurnal variation decays with height so that when the contributions by all levels in the atmosphere are taken into account the diurnal variation in longwave radiation is only slightly more than 6 W $m^{-2}$. A similar pattern is observed in the SPCZ-East region (region 2). Note that the maximum longwave emission occurs at around 0900 LST in the SPCZ region, in good agreement with the results from the NOAA data shown in Fig. 1. Note, however, that Fig. 10 shows evidence of a strong semidiurnal component.

In the ITCZ-regions (3 and 6) where the convection is less active, the contributions to the diurnal variation in emission come from lower levels. There is also less compensation by very high clouds. Again the phase of the diurnal harmonic inferred from the GOES data is consistent with that of the NOAA polar orbiter data

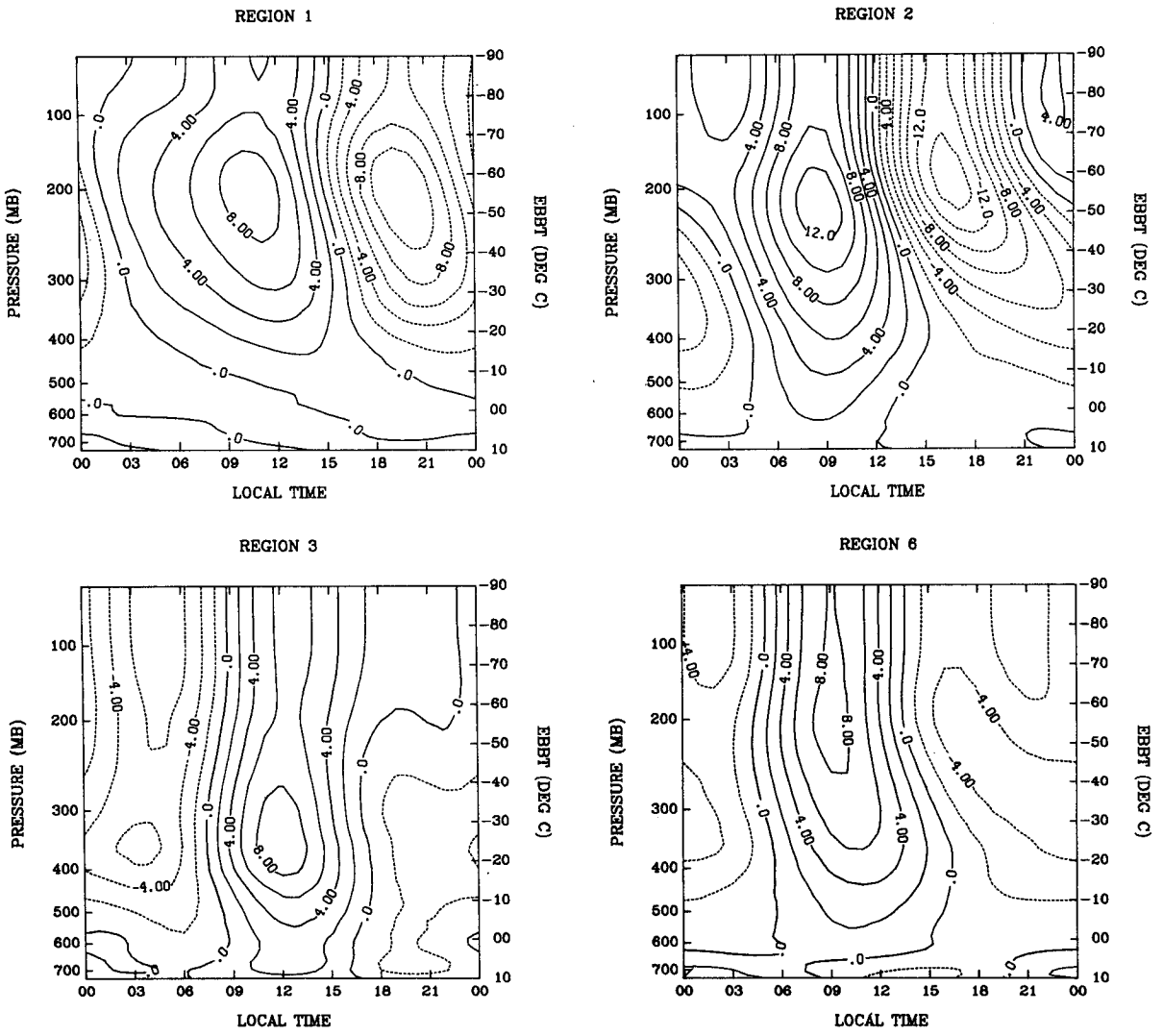


FIG. 10. Diurnal variation in the emitted flux density which would result if only GOES-West pixels with temperatures equal to or warmer than the indicated values of blackbody temperatures are included. [See (10) for formulation.] Contour interval is 2 W $m^{-2}$; negative contours are dashed.

shown in Fig. 1. In the ITCZ-East region (region 3) a clearly defined noon maximum in emission is seen in both data sets. Figure 9 shows that this results from a noontime minimum in clouds below 350 mb.

## 4. Summary and discussion

The diurnal harmonic in outgoing longwave emission in the tropical belt, 30°N–30°S, has been determined from nine years of NOAA polar-orbiting satellite observations. Large diurnal variations with maximum emission near noon are observed over most land areas. Over dry land areas this variation is primarily due to the daytime warming of the surface by solar radiation. Over land areas with intense convection the maximum shifts to before noon because of an evening maximum in deep convective clouds. Over oceanic regions where stratus clouds are known to predominate, a middle to late afternoon maximum in emission is observed. The amplitude is generally less than 5 W $m^{-2}$ over these regions of oceanic stratus. The early morning minimum in longwave emission is consistent with the expected growth of stratus cloudiness during the nighttime hours and stratus "burnoff" during the day.

TABLE 2. GOES-West regions.

| Region number | Description |
|---|---|
| 1 | SPCZ-West region (170°E–170°W) |
| 2 | SPCZ-East region (170°W–150°W) |
| 3 | ITCZ-East region (170°W–140°W) |
| 6 | ITCZ-West region (170°E–170°W) |

A feature of the diurnal variation in longwave radiation which has not been documented previously is the variation associated with well-developed convection over the oceans. It is clear from histograms of both the NOAA 250-km average data and GOES-West 8-km pixel data that the diurnal variation in longwave radiation results from diurnal variations in convective cloud. Variations in convective cloud over the oceans have previously been noted in the GATE area (e.g., Gruber, 1976; Reed and Jaffe, 1981) and a diurnal modulation in tropical storm intensity was observed by Browner et al. (1977). The mechanism responsible for these diurnal variations in cloudiness at locations far removed from land has not been identified, but several possibilities have been offered by McBride and Gray (1980) and Ackerman and Cox (1981).

The GOES data show that in regions of intense convection the coldest clouds (~100 mb) have a diurnal variation which is 180 deg out of phase with the diurnal variation in convective cloud at lower levels (~400 mb). As a result, the amplitude of the diurnal variation in longwave emission is less than would be expected based on the diurnal variation in clouds below 200 mb alone. The diurnal variation in longwave emission over the regions of intense oceanic convection is thus a weak reflection of more substantial diurnal variations in cloud type in these regions.

The variations in outgoing longwave radiation determined from the NOAA 2.5-deg latitude–longitude resolution data and the GOES-West 8-km resolution data are consistent with each other and with diurnal variations in precipitation observed at small islands and atolls in the Pacific. Both satellite data sets indicate that a maximum in longwave emission associated with a minimum in cloudiness occurs between 0600 and 1200 LST. This result is consistent with a minimum in precipitation that is observed at islands along the SPCZ such as Canton Island and French Polynesia (Gray and Jacobson, 1977; see also Albright et al., 1985). These precipitation data often show a strong semidiurnal component, however, which we are unable to resolve with our NOAA multiyear data set because of aliasing by interannual variability.

It is interesting to note that the histograms based on averages over 2.5 × 2.5-deg latitude–longitude boxes provide the same qualitative insight into the diurnal variations in cloudiness as do the 8-km resolution data. This suggests that the gross statistics of clouds and longwave emission are not sensitive to spatial averaging. It seems that at some point spatial averaging will begin to obscure interesting emission variations associated with changes in cloud amount. A comparison of Figs. 3–8 and Fig. 9 suggests, however, that the loss of information in going from 8 km to 250 km is not as great as might be feared. If further study confirms this insensitivity of emission statistics to spatial averaging, then confidence in using averaged products will be increased. On the other hand, substantial loss of important geographical detail in time averages occurs in going from 2.5 × 2.5 to 4.5 × 4.5-deg latitude–longitude resolution.

*Acknowledgments.* We would like to thank M. D. Albright and R. J. Reed for providing the GOES data and for useful discussions. This work was supported by the National Aeronautics and Space Administration, under Contract NAS1-16462.

## REFERENCES

Ackerman, S. A., and S. K. Cox, 1981: GATE Phase III mean synoptic-scale radiative convergence profiles. *Mon. Wea. Rev.*, **109,** 371–383.

Albright, M. D., E. E. Recker, R. J. Reed and R. Dang, 1985: The diurnal variation of deep convection and inferred precipitation in the central tropical Pacific during January–February 1979. *Mon. Wea. Rev.*, **113,** 1663–1680.

Browner, S. P., W. L. Woodley and C. G. Griffith, 1977: Diurnal oscillation of the area of cloudiness associated with tropical storms. *Mon. Wea. Rev.*, **105,** 856–864.

Duvel, J. P., and R. S. Kandel, 1985: Regional-scale diurnal variations of outgoing infrared radiation observed by METEOSAT. *J. Climate Appl. Meteor.*, **24,** 335–349.

Fravalo, C., Y. Fouquart and R. Rosset, 1981: The sensitivity of a model of low stratiform clouds to radiation. *J. Atmos. Sci.*, **38,** 1049–1062.

Gray, W. M., and R. W. Jacobson, Jr., 1977: Diurnal variation of deep cumulus convection. *Mon. Wea. Rev.*, **105,** 1171–1188.

Gruber, A., 1976: An estimate of the daily variation of cloudiness over the GATE A/B area. *Mon. Wea. Rev.*, **104,** 1036–1039.

——, and A. F. Krueger, 1984: The status of the NOAA outgoing longwave radiation data set. *Bull. Amer. Meteor. Soc.*, **65,** 958–962.

Jacobowitz, H., R. J. Tighe and the Nimbus-7 Experiment Team, 1984: The earth radiation budget derived from the Nimbus-7 ERB Experiment. *J. Geophys. Res.*, **89,** 4997–5010.

Liebmann, B., and D. L. Hartmann, 1982: Interannual variations of outgoing IR associated with tropical circulation changes during 1974–78. *J. Atmos. Sci.*, **39,** 1153–1162.

McBride, J., and W. M. Gray, 1980: Mass divergence in tropical weather systems. Paper II. Large-scale controls on convection. *Quart. J. Roy. Meteor. Soc.*, **106,** 517–538.

Minnis, P., and E. F. Harrison, 1984a: Diurnal variability of regional cloud and clear-sky radiative parameters derived from GOES data. Part I: Analysis method. *J. Climate Appl. Meteor.*, **23,** 993–1011.

——, and ——, 1984b: Diurnal variability of regional cloud and clear-sky radiative parameters derived from GOES data. Part II: November 1978 cloud distributions. *J. Climate Appl. Meteor.*, **23,** 1012–1031.

——, and ——, 1984c: Diurnal variability of regional cloud and clear-sky radiative parameters derived from GOES data. Part III: November 1978 radiative parameters. *J. Climate Appl. Meteor.*, **23,** 1032–1051.

Raschke, E., and W. R. Bandeen, 1970: The radiation balance of the planet Earth from radiation measurements of the satellite Nimbus II. *J. Appl. Meteor.*, **9,** 215–238.

Reed, R. J., and K. D. Jaffe, 1981: Diurnal variation of summer convection over West Africa and the tropical eastern Atlantic during 1974 and 1978. *Mon. Wea. Rev.*, **109,** 2527–2534.

Short, D. A., and J. M. Wallace, 1980: Satellite-inferred morning-to-evening cloudiness changes. *Mon. Wea. Rev.*, **108,** 1160–1169.